Selection and experimental evaluation of low-cost porous materials for regenerator applications in thermoacoustic engines

Abdulrahman S. Abduljalil, Zhibin Yu and Artur J. Jaworski [1]

School of Mechanical, Aerospace and Civil Engineering, University of Manchester,
Sackville Street, PO Box 88, Manchester M60 1QD, United Kingdom

[1] Corresponding author, Tel: +44 161 275 4352, Fax: +44 705 360 4497, E-mail: a.jaworski@manchester.ac.uk

ABSTRACT: This paper aims at evaluating three selected low-cost porous materials from the point of view of their suitability as regenerator materials in the design of thermoacoustic travelling wave engines. The materials tested include: a cellular ceramic substrate with regular square channels; steel "scourers"; and stainless steel "wool". Comparisons are made against a widely used regenerator material: stainless steel woven wire mesh screen. For meaningful comparisons, the materials are selected to have similar hydraulic radii. One set of regenerators was designed around the hydraulic radius of 200 μm. This included the ceramic substrate, steel "scourers", stainless steel "wool" and stacked wire screens (as a reference). This set was complemented by steel "scourers" and stacked wire screens (as a reference) with hydraulic radii of 120 μm. Therefore six regenerators were produced to carry out the testing. Initial tests were made in a steady air flow to estimate their relative pressure drop due to viscous dissipation. Subsequently, they were installed in a looped-tube travelling-wave thermoacoustic engine to test their relative performance. Testing included the onset temperature difference, the maximum pressure amplitude generated and the acoustic power output as a function of mean pressure between 0 and 10 bar above atmospheric. It appears that the performance of regenerators made out of "scourers" and steel "wool" is much worse than their mesh-screen counterparts of the same hydraulic radius. However cellular ceramics may offer an alternative to traditional regenerator materials to reduce the overall system costs. Detailed discussions are provided.

Keywords: E: thermal; G: thermal analysis; H: selection for material properties

1. Introduction

In thermoacoustic engines, thermal energy is directly converted to an acoustic wave (mechanical energy) as a result of heat interaction between a solid material and adjacent gas, within the so-called "thermal penetration depth". This is based on a well-known thermoacoustic effect that was first explained qualitatively by Lord Rayleigh: "if heat be given to the air at the moment of greatest condensation, or be taken from it at the moment of greatest rarefaction, the vibration is encouraged" [1] and is known today as "Rayleigh criterion" [2] (which can also be expressed mathematically). The potential of the thermoacoustic effect went unrecognised until Rott [3,4] established its theoretical foundations based on the linear thermoacoustic theory. Later, Ceperley [5] recognised that when a travelling sound wave passes though a porous material (regenerator), the heat transfer interaction between the gas and the solid material causes the gas to undergo a Stirling-like thermodynamic cycle. This led to construction of many prototype thermoacoustic engines and refrigerators, where the main component is the so called "thermoacoustic core" comprising a porous solid material (a stack in the standing wave devices or a regenerator in the travelling wave devices) and a pair of heat exchangers ("hot"

and “cold”) to provide the required temperature conditions on the ends of the porous medium for the thermoacoustic effect to take place.

A detailed theoretical analysis of standing wave systems, based on the linear acoustics model was performed by Swift [6], who also provided some examples of the early developments at Los Alamos National Laboratory. He also provided a detailed analysis of a practical standing-wave engine where 7000 W of thermal energy was converted to 630 W of acoustic power [7]. Studies of a somewhat different symmetrical double-ended system have been reported by Olson and Swift [8]. Zhou and Matsubara [9] studied the performance of a standing wave engine as a function of gas properties, frequency, mean pressure, stack length and the hydraulic radius of the mesh used to fabricate the stack. They also expressed the engine performance in terms of the normalised input power, hot heat exchanger temperature and measured pressure amplitudes.

Following his earlier work [5], carried out for infinite regenerators, Ceperley [10] provided further theoretical insights into the workings of travelling wave engines equipped with short regenerators and demonstrated that one of the key parameters for obtaining high efficiencies is the regenerator acoustic impedance. Following Ceperley’s ideas, a torus (looped-tube) travelling-wave engine, with the torus length equal to the wavelength of the fundamental acoustic mode of the engine, became one of the common configurations for both fundamental research and practical applications (cf. Yazaki et al. [11] or Yu and Jaworski [12]). Backhaus and Swift [13] developed a somewhat different concept of a travelling wave engine, where a torus resonator was connected to a standing wave resonator, which defined the operating frequency, while de Blok [14] proposed a novel hybrid configuration with a travelling wave feedback waveguide. A more detailed review of various types of travelling wave engines has been recently given by Yu and Jaworski [15].

Figure 1 shows a typical configuration of the travelling wave thermoacoustic engine; green arrows marking the acoustic power flow. Here, the thermoacoustic core works as a power amplifier. To complete the thermodynamic process in the regenerator, the acoustic power has to be supplied to the ambient (cold) end of the regenerator with a near travelling-wave phasing. Therefore, either an external acoustic source [16,17] or a feedback mechanism needs to be designed [11,13,18] to feed the acoustic power into the ambient end of the regenerator. The characteristics of the regenerator determine the performance of the travelling-wave thermoacoustic engine in two respects. Firstly, the local acoustic impedance at the cold end of the regenerator determines how large an acoustic power flux can be fed into the regenerator. The impedance values are generally determined by the acoustic network which consists of the acoustic compliance, inertance tube and the flow resistance in the regenerator. Of course, higher impedance will result in a lower acoustic power being fed into the regenerator. Secondly, in the regenerator, the heat contact between the gas and the solid material determines the thermodynamic process. For the travelling wave thermoacoustic engine, a near isothermal condition is required in the regenerator [11]. To achieve this condition, hydraulic radius, r_h, defined as the ratio of the total gas volume to the gas-solid interface area, should be much smaller than the thermal penetration depth to ensure a very good heat contact between the gas and the solid material. The heat capacity of the solid material should also be large enough for heat transfer between the gas and solid material. On the other hand, flow resistance should be as small as possible to reduce the dissipation.

The potential advantages of thermoacoustic engines are their simplicity of construction and low cost. The costs of an appropriate resonator are relatively low as it can be built of standard metal or plastic tubing; the most costly parts of

such devices are the regenerators and two heat exchangers. Due to the critical nature of the interaction between the gas and solid material forming the regenerators, there have been a number of studies focused on the selection and optimisation of the regenerators for travelling-wave engines. Typically, regenerators with regular geometrical configurations, for example parallel-plate type [15], offer excellent performance: cf. comparative studies [19,20] for instance. However, such regenerators are too costly and too difficult to make, especially when the channel size goes down into tens of microns range. Similarly, there seem to be very few commonly available materials for such regenerators. Therefore, a common practice in thermoacoustics is to use multiple layers of mesh screens stacked together to form a porous structure. This is not ideal because the tortuous gas path causes large viscous losses. Similarly the cost and the labour involved in manufacturing such regenerators are still substantial and may be prohibitive for mass production.

The idea behind the current research is to identify easily accessible materials for a potential application as regenerators, and characterise their performance against one another using a purpose-built travelling wave looped-tube engine as a testing platform. It is envisaged that parameters such as the maximum pressure amplitude generated, the onset temperature difference, the temperature gradient developed in the regenerator and the acoustic power fed into the ambient end of the regenerator can serve as meaningful criteria for selection of regenerator materials for practical applications. This paper gives an account of the selection of regenerator materials for testing, fabrication of the regenerator samples and the design of the experimental facilities, followed by the presentation of results and conclusions. In particular, section 2 gives detailed information about materials used for fabricating the regenerators tested in the current study. This section discusses their geometrical properties such as porosity and hydraulic radius, summarizes the properties of six regenerator samples fabricated and studies their static pressure drop characteristics. Section 3 outlines the construction of experimental apparatus to study the thermoacoustic behaviour of the sample regenerators. Section 4 discusses the results obtained from the point of view of the onset temperature difference, acoustic pressure amplitudes generated, acoustic powers obtained, investigates the temperature gradients developed along the regenerators and discusses the experimental uncertainties. Finally, section 5 presents overall conclusions from the study.

2. Selection, preparation and properties of regenerator materials

The low-cost regenerator materials selected for this study included three types: cellular ceramics, steel “scourers” and stainless steel “wool”, while standard mesh screens were used for benchmarking purposes. The characteristics of the regenerator materials are outlined below.

2.1. Cellular ceramic catalyst support

The first material (denoted as Material/Regenerator I) was made from Corning cellular ceramic catalyst support, which has square channels with cell density of 900 cells per square inch (or 30 cells per linear inch, i.e. 25.4 mm), a hydraulic radius, r_h, of 199 μm and porosity, ϕ, of 88.7%. This type of material is typically used in catalytic converters in the automotive industry. It was considered low cost since a sample of 90mm diameter and 125 mm length (see Fig. 2) was around £50 – thought to be competitive relative to standard wire mesh screens. Unfortunately, when using this type of material one cannot choose the hydraulic radius with the same level of flexibility as wire mesh screens: the ceramic catalyst support comes typically in sizes such as 300, 400, 600 or 900 CPSI. The latter was the finest pore that was

available for this study, which meant that for meaningful comparisons all other materials had to be tested with similar equivalent hydraulic radii of around 200 μm.

2.2. Steel "scourers"

The second material selected for this study is commonly known as steel "scourers" (cf. Figure 4b later). It is a product with predominantly domestic applications for scrubbing and cleaning. A packet of three "handfuls" was only around £1, which meant that the whole regenerator material for this study would be within £5 price range. The structure of this material can be imagined as metal "swarf" (metal cuttings from metal turning operations) with relatively uniform rectangular cross-section (with typical dimensions 400-500 μm by 20-30 μm), which is subsequently formed into "disks" that fit the human palm. As this is a material of "random structure", to control the hydraulic radius one needs to carefully press the material to a desired bulk density (or porosity), while taking into account the actual average cross section of the "rectangular wire".

From first principles, the hydraulic radius is defined in thermoacoustics [21] as the ratio of the total gas volume to the gas-solid interface area (commonly referred to as "wetted area"). Assuming that a single wire of cross-sectional area A_{cs}, perimeter P, length L and density ρ_{solid} is pressed into a regenerator of a known volume V_{reg}, it is easy to show that the desired hydraulic radius must be:

$$r_h = \frac{V_{gas}}{A_{wetted}} = \frac{V_{gas}}{PL} = \frac{A_{cs}}{P}\frac{V_{gas}}{A_{cs}L} = \frac{A_{cs}}{P}\frac{V_{gas}}{V_{solid}} = \frac{A_{cs}}{P}\frac{\phi}{1-\phi} \tag{1}$$

or in other words

$$\phi = \frac{r_h}{r_h + \frac{A_{cs}}{P}}. \tag{2}$$

However porosity, ϕ, is by definition

$$\phi = \frac{V_{gas}}{V_{reg}} = \frac{V_{reg} - V_{solid}}{V_{reg}} = \frac{V_{reg} - \frac{m_{solid}}{\rho_{solid}}}{V_{reg}}. \tag{3}$$

Of course, the volume of the regenerator is the sum of the volumes of the gas and solid, $V_{reg} = V_{gas} + V_{solid}$, and m_{solid} is mass of the solid material. A_{wetted} is the "wetted area" equal PL for the wire.

Comparing (2) and (3) it is easy to show that the required mass of the solid material is

$$m_{solid} = V_{reg}\rho_{solid}\frac{A_{cs}}{A_{cs} + r_h P}. \tag{4}$$

For the "rectangular wire" (such as "scourers discussed here) of the characteristic cross-sectional dimensions *a* and *b*, the cross-sectional area and perimeter are *ab* and *2(a+b)*, respectively and equation (4) simplifies to

$$m_{solid} = V_{reg}\rho_{solid}\frac{ab}{ab + 2r_h(a+b)}. \quad (5)$$

To find average values of *a* and *b*, around 100 samples have been measured for each package of scourers. The measured averaged dimensions were approximately 432 μm x 25.6 μm. Two hydraulic radii were investigated for scourers: 200 μm, in order to make comparisons with the ceramic material, and 120 μm – with the hope to shift the optimum mean pressure towards higher pressures and compare the performance with scourers of 200 μm hydraulic radius. Scourers compressed to provide r_h = 200 μm are referred to as Material/Regenerator II-a, while those compressed to provide r_h = 120 μm are referred to as Material/Regenerator II-b.

2.3. Stainless steel "wool"

The third low-cost material studied here was the so called stainless steel "wool". It is also used in domestic applications (e.g. wooden parquet scrubbing) or industrially (e.g. to clean and roughen surfaces before soldering). The grade acquired for this investigation was S/S 434 with the cost of around £10 per 100g package, which meant that the cost of the steel "wool" regenerator in our rig was around £15. The main difference between "wool" and "scourers" is the wire structure: "wool" wires are not uniform in cross-sectional shape and size. In order to obtain the desired mass per unit volume (for the compression process) one needs to characterise the average properties of "wool" wires first.

To this end a sample of around 300 individual wires were chosen in as random fashion as possible. These were straightened and cut to a common length and subsequently aligned in one direction. An epoxy-type material was cast around them to form a cylindrical mould; the individual wires having been placed as parallel to the cylinder axis as possible. Subsequently a central section of the cylinder was cut out and its end surfaces polished to reveal wires' cross-sections for microscope imaging in order to extract their cross-sectional areas and perimeter lengths. Figure 3a shows the wire wool material, while Fig. 3b shows the sample wires cast in a cylindrical mould. Images were taken under a microscope, maintaining a known scale at various positions of the cut plane to maximize the number of samples for measurement. Figure 3c shows a raw image obtained from the microscope: white areas are the wire cross-sections while the grey background is the polished epoxy matrix.

MATLAB code was developed to extract the necessary information from the images. These are 8-bit (0-255) greyscale JPG images, with the size of 1030 × 1300 pixels. As a first step, any white area (i.e. the wire-cross section) that did not show completely because of its position close to the edge of the image was removed manually The images were then converted to black and white: A greyscale threshold of 175 was set so that any value less than or equal 175 was regarded as "black" (0), and any value larger than 175 was regarded as "white" (255). The threshold value was selected experimentally by "trial and error": a set of sample images was converted using varied levels of threshold and the resulting images were compared visually to the originals from the point of view of consistency of shapes and sizes of

the wire cross-sectional areas. The images obtained using the threshold value of 80 seemed to produce the best black and white representation of the original images. The resulting black and white image is shown in Figure 3d.

Subsequently, the cross-sectional area of the wires could be calculated from the number of white pixels within each shape, knowing the linear scaling factor (i.e. how many pixels per mm). A scale of 1 mm is given in the original image, from which the scaling factor is worked out and it remains the same for all images. It is also possible to apply suitable filters to extract the wire circumference: when a pixel has a white and black neighbour, in either horizontal or vertical direction, it is counted as a point "on the circumference", and is set to white. The rest was set to black. This is illustrated in Fig. 3e. The topology of the white pixels is such that they form a continuous line with two types of neighbourhood: "side-to-side" or "corner-to-corner". The circumference is calculated by a procedure that can be described as a "walk" around the circumference and summing the distances between "visited" pixels: unity for "side-to-side" neighbours and square root of 2 for corner-to-corner neighbours. The procedure was validated for a few known shapes (circles, rectangles, diamonds end) and a selected random shape that was magnified and the circumference measured by a piece of string along the edge. The discrepancies were no more than 2%. Summation of calculated areas and perimeters (circumference lengths) over all samples allowed obtaining their average values, which turned out to be 4570 μm^2 and 249 μm, respectively.

In order to calculate the mass of steel wool required to build a regenerator of predefined hydraulic radius one needs to apply the general equation (4). Only one hydraulic radius was considered for steel wool regenerator, namely 200 μm. Steel wool regenerator is referred to as Material/Regenerator III.

2.4. Wire Mesh Screens

For comparative studies, standard wire mesh screens were used as regenerator material. For wire mesh screens, the relationship between the hydraulic radius r_h, wire diameter D_{wire} and porosity ϕ (Eq. (1)) can be re-written as

$$r_h = D_{wire} \frac{\phi}{4(1-\phi)}. \tag{6}$$

For a given mesh screen, the wire diameter and the so called "mesh number" n, are provided by the manufacturer. The porosity can thus be calculated as:

$$\phi = 1 - \frac{\pi n D_{wire}}{4} \tag{7}$$

Two wire mesh screen materials were selected. The first was to match the hydraulic radius of 200 μm. Here mesh number n = 30 was selected, with the wire diameter of 280 μm, which resulted in the hydraulic radius of 196 μm. The second was to match the hydraulic radius of 120 μm. Here mesh number n = 45 was selected, with the wire diameter of 230 μm, which resulted in the equivalent hydraulic radius of 121 μm. Both wire mesh materials were purchased in the form of 50 mm disks, which had to be subsequently stacked together to form the regenerators. Wire mesh screen

regenerators are referred to as Material/Regenerator IV-a and IV-b, for the nominal hydraulic radii 200 μm and 12 μm, respectively.

2.5. Summary of materials used and fabrication of regenerators

Table 1 gives a summary of all materials used to construct regenerators for the current study, while Fig. 4 shows images of the actual regenerator assemblies for the main four types of regenerators. Insets at the bottom are close-ups of actual materials.

All of the regenerators used in this study were designed to the same size: 100 mm length and diameter to fit the internal diameter of the rig: 56 mm. There was only one small difference introduced for practical reasons of handling the thermocouple insertion: materials I, II and III were inserted into purpose designed metal cans (as seen for example in Fig. 4b) of the internal diameter 54 mm and 1 mm wall thickness, while the wire mesh screen regenerators were built directly inside the 56 mm pipe forming the rig.

Fabrication of regenerator I was relatively straightforward: the ceramic material was cut to size using a hand saw. In addition 3 holes were drilled from the side to introduce thermocouples (see section 3). Compacting random materials of type II and III required a special tool (a "stamp") to be made to control the applied pressure. A series of disks (such as seen in the inset of Fig 3c) would be manufactured first, and these would be subsequently placed inside the metal cans. The mass of scourers to build regenerator II-a was 121 g, while it was 164 g for regenerator II-b. The mass of steel "wool" required to build regenerator III was 154 g. Metal cans containing the regenerator materials would be placed inside the rig test section as illustrated in Fig. 4c. Regenerator IV-a was fabricated by compacting together 182 disks of 50 mm diameter cut out from the wire mesh sheet. An additional rectangular sheet was wound around the assembly to fill in the gap between the disks and the inner pipe wall. This assembly is shown in Fig. 4d. Regenerator IV-b was made in the same way, except that 201 discs were used because the wire diameter is smaller.

As already mentioned, the objective of the experiments was to investigate the performance of the regenerators while keeping the hydraulic radius constant (200 μm or 120 μm). The particular materials and wire geometries used in the study meant that it was not possible to keep porosities the same at the same time. Clearly the wire mesh screens have porosities of about 70%, while the scourers and wire wool can only achieve porosities of 90.7 – 94.2%. Increasing the mass and packing of this material within the can could lower the porosity, but as will be clear from the static pressure drop measurements it would render the regenerators too lossy for the engine to start. Theoretically, it could be feasible to choose different wire sizes to try to match both the hydraulic radius and the porosity to those of wire mesh screens, but this was not achieved in the current work.

2.6. Viscous Losses in Regenerators

Viscous resistance plays an important role in the regenerator of a travelling wave thermoacoustic engine. Higher flow resistance leads to higher viscous losses and causes a higher local acoustic impedance in the regenerator, which reduce the acoustic power feedback [15]. The flow resistance of the regenerator can be tested in either oscillatory flow [22,23] or steady flow [19,24]. In this research, before the actual experiments aiming at characterising the thermoacoustic performance of regenerators, they were all subjected to a static pressure drop test under steady flow conditions, in order

to obtain some estimates of their viscous dissipation [19]. To this end, a simple rig was constructed whose main part is a 2.2 m long PVC tube with the outside diameter of 60.3 mm, and inside diameter of 56 mm (see Fig. 5). The tube is equipped with purpose made fittings to accommodate the regenerator cans. Static pressure ports allow measuring the pressure drop across the regenerator (micro-manometer 1) while a Pitot-static tube provides simultaneous velocity measurements (micro-manometer 2). The tube is attached to a 20kW centrifugal blower. This arrangement had no speed control, but the use was made of very long turn-down times of the selected centrifugal fan (of the order of minutes) which allowed quasi-steady measurements. The fan was started at its maximum power, which yielded the maximum values of the air speed and the corresponding pressure drop across the regenerator. Then, the fan was turned off and video recording of the measurement readouts of the two instruments was made. The data points were simply extracted from the video recordings. Three runs were made for each regenerator and average values of pressure drop vs. velocity are plotted in Fig. 6. As the fan takes a long time to slow down, the manometer and the connecting tubing can follow the transients. The results shown in Fig. 6 are quite similar with those shown in Refs [19] and [24]. It can be found that the flow resistance depends on porosity, regularity or the porous material, and the nature of packing of the solid materal: the lower the porosity the higher the flow resistance. A higher flow resistance and a nonlinear relationship between the pressure drop and velocity were observed when materials are more random.

3. Experimental setup – design and construction of the looped-tube engine for regenerator testing

The experimental apparatus to test the performance of regenerators described in section II is shown in Fig. 7. Figure 7a outlines the basic concept: the rig is essentially a travelling wave looped tube engine with the thermoacoustic core installed in a selected location along the loop. Air is used as the working gas; the design frequency is 110 Hz. As shown in Fig 7b, the system is made of stainless steel piping with the total length of 306 cm and an internal diameter of 56 mm. All flanges are ASME grade 316L and class 300. The resonator has a constant cross-sectional area throughout. The system was designed to handle a mean pressure of up to 1.2MPa and a maximum temperature of 750°C in the hottest zone of the tube (brown discolouration of one of the flanges indicates the location of the heater – cf. Fig. 7b). The regenerator and the hot and cold heat exchangers are shown schematically in Fig. 7a, while Figs. 7c and 7d show the images of the actual hot and cold heat exchanger assemblies.

The hot heat exchanger is made in the form of an electric heater that was purpose made to supply a uniform heat flux to one end of the regenerator. It was made from Nickel-Chromium resistance wire which was wound around ceramic tubes that serve as supports. Electrical power is supplied to the heater at a maximum voltage of 30V and a maximum current of 20A from a DC power supply via a special feed-through to maintain a good pressure seal. The cold heat exchanger is made using a set of 6 stainless steel tubes (O/D 6 mm) protruding through the main engine duct wall and passing through a car radiator matrix fitted on the inside. A good fit of the tubes within the car radiator matrix allows a good heat transfer by conduction between the matrix and the tubes.

The engine is instrumented with seven type-K thermocouples (TC-Direct model 408-119), which are used to measure the gas temperature along the centre of the regenerator (numbered 1 through to 5 – see Fig 7a) and within the two heat exchangers (thermocouples numbered 0 and 6, for hot and cold heat exchangers, respectively). TC-Direct fittings (model 875-446) were used to feed the thermocouple wires through the tube wall, to ensure a good pressure seal. The thermocouples were spread evenly along the regenerators, except T2 (cf. Fig 7a), which was placed 33 mm from the hot

end of the regenerator (instead of the expected 25 mm). This was because of the particular flange arrangement within the rig.

A pair of high pressure microphones (PCB PIEZOTRONICS, INC., USA; model 112A22) is used to measure the oscillating pressure amplitudes as well as the phase angle between the two received signals from the transducers. Symbols P-A and P-B in Fig.7a mark the locations of the two microphones. Starting from the end of the cold heat exchanger and counting along the centreline of the acoustic duct (see coordinate x in Fig. 7a) the positions of sensors A and B are 38 and 147.5 cm, respectively. The sensitivity of the sensors is 100mV/psi.

4. Experimental results and discussion

Performance of the engine equipped with six regenerators described in section II was tested in two ways. Firstly, starting from the situation when the rig was at room conditions, the engine onset temperature was established by exciting the hot heat exchanger (by supplying 435 W of electrical energy into the resistance wires) and observing the temperature difference between the hot and cold end of the regenerator required for establishing the acoustic excitation. This procedure was repeated for a range of mean gas pressures (between 0 and 150 psi gauge, typically in 5 or 10 psi steps). After each experiment the engine's temperature was brought down to the room temperature to allow comparable conditions for the next experiment. It should be noted that the electrical power input was ramped up to the maximum value instantaneously at the start of each onset temperature experiment (and not increased gradually). Usually, this will cause a nonlinear temperature profile along the regenerator. However, setting the input power directly to the required power rate is more practical because a quick engine start-up is favourable for any practical thermoacoustic engines. Figure 8 illustrates the readings from thermocouples 1 – 5 for Regenerator I, at mean pressure of 4.4 bar obtained during the engine start-up.

Secondly, the pressure amplitude achieved by the engine in a steady state was used as a measure of regenerator's performance. As the research in this paper is still a preliminary investigation, no acoustic load is connected to the engine to extract acoustic power out from the engine. However, it is well-known that in the absence of the acoustic load, all of the acoustic power will be dissipated on the internal surfaces of the resonator. Furthermore, the acoustic power flow in the resonator is proportional to the square of the pressure amplitude. In this respect, it is possible to just use the pressure amplitude as a simple performance indicator. The pressure amplitude was obtained as a function of the mean pressure of the working gas. Finally, for each steady state condition, acoustic power at the point half-way between sensors P-A and P-B was measured using a standard two-microphone method [25]. In addition to the above engine performance indicators, temperature gradient along the regenerator was investigated to ascertain whether the acoustic power production was uniform within the regenerator (i.e. whether the whole of the regenerator length contributed equally to the acoustic power generation).

4.1. Onset temperature difference studies

Onset temperature difference, understood as the minimum difference between the temperatures of the hot and cold ends of the regenerator necessary to induce the engine's self-oscillations, is one of the basic parameters for thermoacoustic engines [11]. The onset temperature can be plotted as a function of the mean pressure of the working gas, which is the classic stability curve for the thermoacoustic engines [26,27]. In this way, the optimal mean pressure corresponding to

the lowest onset temperature differences can be found experimentally. In practice, a low onset temperature difference is advantageous, especially for engines driven by low temperature heat sources. Figure 9 shows the experimental data obtained for all regenerators tested.

From Figure 9 it can be seen that Regenerator I has the minimum onset temperature difference, ΔT_{onset}, of about 350 K, within pressure range of 2.5–4.5 bar; the stability curve having two distinct branches. For the convenience of further discussions the mean pressure corresponding to the minimum ΔT_{onset} will be denoted $P_{m,opti}$. For the left branch of the minimum onset temperature difference curve, the regenerator operates in the near-isothermal zone [11,27]. The mean pressure is relatively low, and the thermal penetration depth is much higher than the hydraulic radius. However, for the right branch, the mean pressure is relatively high and the thermal penetration depth relatively small. The regenerator works in the near adiabatic region [11,27]. For Regenerator II-a this trend is repeated only partially. There seems to be a local minimum ΔT_{onset} for around 3–3.5 bar. However the right branch, experiencing a slight rise at first, drops down for pressures higher than 5 bar (this would apparently indicate an easier start-up). However, for pressures higher than about 6.5 bar it is not possible to start the engine at all.

Regenerator II-b exhibits a similar behaviour to II-a: a local minimum at 3 bar, followed by a rise and fall as mean pressure increases. Subsequently, the curve is discontinued after reaching the pressure of 8.5 bar (no start-up possible). However, most importantly the required temperature difference to start the engine is substantially higher than for regenerators I and II-a: namely in the range 720–790 K, making it an unlikely candidate to apply in realistic systems. The second drop of the onset temperature difference after the mean pressure reached 6 bar indicates that the stability curves of Scourers Regenerators II-a and II-b have different characteristics compared to those made out of mesh screens or ceramic material. Such a comparison is also true when comparing these results with the ones reported in Refs [11] and [28]. The shape of the stability curves for Regenerators II-a and II-b may indicate that the properties such as the hydraulic radius and porosity in these two regenerators are somewhat inhomogeneous. Although the scourers are compressed into the can carefully, the nature of this material is very random and non-uniform material distribution is likely. In addition it is possible that for random materials a concept of a “single” hydraulic radius is not reasonable: pore sizes have inevitably a continuous distribution and various length-scales may become dominant at different mean pressures, resulting in local minima or maxima of the stability curves.

Regenerator III (as far as can be ascertained from the data points available) also exhibits a classic behaviour with two branches of the stability curve. $P_{m,opti}$ is relatively high: around 9 bar. The left branch of the curve begins at pressure of about 2.5 bar (below 2.5 bar no start-up is possible) with relatively high ΔT_{onset} (around 770 K), but subsequently drops rapidly, so that reasonable levels of ΔT_{onset} are assumed for pressures above 5 or 6 bar. It looks as though the right branch of the curve begins for $P_{m,opti}$ around 9 bar, but unfortunately the experiments cannot be continued beyond 11.5 bar due to the pressure rating limitations of the experimental rig.

Compared to the low-cost materials, the benchmark Regenerator IV-a seems to follow the classic stability curve (left and right branches), with a somewhat ill-defined $P_{m,opti}$ between 4 and 5 bar. However, it is clear that the onset temperature difference is the lowest of all materials tested, up to around 9 bar. Beyond 9 bar, the performance of steel wool (Material III) seems to be better, as is the performance of the other benchmark material IV-b.

Regenerator IV-b seems to only have the "left" branch of the onset temperature difference curve. This means that the hydraulic radius is relatively small compared to its optimum value, within the tested pressure range. As a result, the regenerator works in the near isothermal region for the whole tested pressures. It needs a higher mean pressure to approach the minimum onset temperature difference and the near adiabatic region, which is outside the certified pressure range of the engine. Furthermore, within most of the pressure range, ΔT_{onset} for Regenerator IV-b is larger than that of Regenerator IV-a (except in the range 9–11.5 bar). However, Regenerator IV-b performs better than any of the low-cost materials, as far as the onset temperature is concerned.

4.2. Pressure amplitude comparisons

Figure 10 shows the measured pressure amplitudes for each regenerator in the tested mean pressure range. Here, the pressure amplitude is defined as half of the peak-to-peak pressure oscillation. From Fig. 10 it can be found that the amplitude curves for Regenerators II-a, II-b, IV-a and VI-b are very similar in character. They start at low amplitudes for low mean pressures, increase almost monotonically with pressure, until they reach a local maximum, after which point their performance drops abruptly (except Regenerator IV-a, for which the curve is monotonic until the end of the pressure measurement range). Out of these four Regenerators the highest amplitudes are generated for IV-a, followed by VI-b, II-b and II-a, respectively. In the same sequence, the cut-off pressure after which the amplitude drops abruptly is getting lower (not identifiable for IV-a, 10 bar for IV-b, 8 bar for II-b and 5.5 bar for II-a).

In essence, the working condition in the regenerator can be adjusted by varying the mean pressure. A higher mean pressure leads to a thinner thermal penetration depth, δ_k. As a result, the ratio δ_k/r_h can be controlled in the regenerator. The previous researches showed that the travelling wave thermoacoustic engine can achieve the best performance when $\delta_k/r_h = 4 - 7$ [29]. Therefore, either very low or very high mean pressure will cause δ_k/r_h to fall far away from the optimal region and lead to a lower pressure amplitude as shown in Fig. 10. However, for Regenerator I and IV-a, there is only one branch obtained and this is likely to be caused by the tested pressure range not being wide enough.

As shown in Table 1, the regenerators discussed above have almost the same hydraulic radius, however their porosities are quite different ("scourers" having significantly higher porosities). Comparing Fig. 9 with Fig. 10, one can find that the regions of decreasing pressure amplitude correspond to the near-adiabatic region. Generally, the heat relaxation loss dominates in these near-adiabatic regions. It can be inferred that the porosity is too high, which leads to very low mass of the solid material, as well as the heat capacity in the regenerator. A very low heat capacity of the solid material will cause high heat relaxation loss and a decrease in performance. However, it needs to be remembered that there are very many other parameters potentially responsible for the large performance differences observed, and so it may not be possible to pinpoint a single reason.

Interestingly, steel "wool" (III) follows a similar trend in the shape of the curve. It starts as the worst regenerator, but above 6 bar becomes better than IV-b, and after 9 bar becomes the best regenerator from the point of view of the produced pressure amplitude. This seems to mirror very well its onset temperature characteristics.

The behaviour of Regenerator I is somewhat different than the rest. The curve is relatively flat, starting from 7 kPa at 1.5 bar, raising to 9 kPa for 5 bar, and dropping down to 8 kPa, by the time the pressure reaches 9 bar. It is worth pointing out that this is the only "regular geometry" regenerator used in this study, with a relatively small pressure drop,

hence it is possible that it operates relatively well across a wider range of pressures (albeit not being the best across the whole range of regenerators.

4.3. Comparisons of acoustic power

Further analysis of the regenerators' performances is based on investigating the acoustic power flow running through the resonator. This acoustic power flow is known as loop-power [14]. As mentioned above, two pressure sensors (as indicated by P-A and P-B in Fig. 7a) have been used to measure the pressures along resonator. The signals of these two sensors are recorded by the data acquisition card simultaneously, giving both their amplitudes and relative phase shift. Using the known distance between the two pressure sensors, the acoustic power passing through the middle point between P-A and P-B can be estimated using the two-microphone measurement method [25] (the details of which are omitted here). The estimated acoustic power for the tested cases is shown in Fig. 11.

Results in Fig. 11 can be interpreted on an approximate level as the acoustic power fed back to the cold end of the regenerator. As mentioned in the introduction, the magnitude of the power feedback and the temperature gradient through the regenerator determines the power output of the regenerator. In this respect, it can also reflect the performance of the regenerator. From Fig. 11, it can be inferred that the behaviour of four Regenerators: II-a, II-b, IV-a and IV-b is again somewhat similar in an overall character. The curves start at low pressure with relatively low power levels, but grow rapidly and subsequently level off. This "plateau" is disrupted by a sudden drop at pressures corresponding to amplitude drops in Fig. 10. Of course the power levels for the four regenerators are different, Regenerator IV-a being best, followed by IV-b, with II-a and II-b producing only fraction of the power of the other two. Regenerator III does not follow the above trend exactly: the rise in power is relatively monotonic, and by the time the pressure of 9 bar is reach the this regenerator outperforms IV-b, but is somewhat worse than IV-a. Similarly as before (cf. Figs. 9 and 10), Regenerator I follows a totally different trend: it starts with high power in low pressure range. The power drops quickly and reaches a local maximum (3.5 bar), followed by a local maximum (5 bar) and subsequently drops monotonically until a cut-off pressure of 9 bar.

The acoustic power feedback is proportional to the pressure amplitude and inversely proportional to the amplitude of the local acoustic impedance at the cold end of the regenerator. Higher flow resistance of the regenerator leads to a smaller acoustic velocity through the regenerator, and as a result, leads to a higher acoustic impedance at the cold end of the regenerator. Therefore, a regenerator with a smaller flow resistance and higher pressure amplitude gives a high acoustic power feedback. Figure 11 can be understood bearing in mind this mechanism. The ceramic regenerator (Regenerator I) has a very small flow resistance (see Fig. 6) and medium pressure amplitude (see Fig. 10). As shown in Fig. 11, it has relatively high acoustic power feedback. Another example is Regenerator II-b, which has a relatively high flow resistance (see Fig. 6), and small pressure amplitude (see Fig. 10). Therefore, it can be found that it has very small acoustic power feedback.

4.4. Regenerator temperature profiles

Further analysis of the regenerators' performances is based on investigating the temperature profiles along the regenerator length in the steady state. The temperature gradient along the centreline of the regenerator was plotted for three selected mean pressures: 3.04 bar, 5.08 bar and 9.16 bar. These are shown in Figs. 12 a–c, respectively.

It can be seen that for these three cases of different mean pressures, the temperature profiles for different regenerators are apparently different. The different temperature profiles along these regenerators can be attributed to many individual reasons or the combination of them. These reasons include regenerator porosity, material properties, flow resistance, the orientation of the rig, the acoustic streaming, and etc. Therefore, the mechanisms behind these different temperature profiles can be quite complicated.

However, here, an attempt is made to investigate how the regenerator porosity, mean pressure and flow resistance affect the temperature profiles. From Fig. 12, it can be found that the temperature distribution along the Regenerator I tends to be more linear compared to other regenerators. This kind of behaviour of the temperature distribution may be related to the porosity of the regenerator and the flow resistance. The rig is mounted vertically, i.e. the heater is below the regenerator. Furthermore, there is no membrane to stop any streaming. In fact, temperature also changes due to the existence of acoustic streaming [30]. The natural convection will be considerable. In fact, in this rig it is helpful to transfer heat from the heater the hot end of the regenerator. As Regenerator I has the highest porosity and the lowest flow resistance, the natural convection effects can propagate much deeper into the regenerator. As a result, the temperature profile is more linear.

In most cases of random materials, the hot end temperature at 3.04 bar seems higher than that for higher pressure of 5.08 bar. This can be explained by the effect of the relatively higher pressure amplitude at this mean pressure, which influences the heat transfer from the heater to the hot end and through the regenerator. On the other hand, they have a very high flow resistance, which leads to a very low acoustic velocity in the regenerator. As a result, heat transport along the axis of the regenerator due to the natural convection and the forced convection by the acoustic displacement cannot reach very deep into the regenerator. Therefore, the temperature distribution has a strongly nonlinear shape. Similarly, the increase of the mean pressure tends to change the temperature gradient towards a more linear shape as the mean pressure increases. Actually, the heat transfer from the heater to the regenerator is also improved due to the increase of the density of working gas. This can explain the fact that higher mean pressure tends to result in a more linear temperature profile.

4.5. Comments on Experiment Uncertainty

A rigorous error analysis in a complex system such as described in this paper is relatively difficult. Of course individual errors of each type of measurement are known (thermocouples, pressure transducers etc.) however the important aspect of the experiments is whether the observed thermoacoustic processes are fully repeatable for the same experimental conditions. A more useful measure of the experimental uncertainty is therefore its repeatability, which gives some indication of the compounded value of measurement error. As a demonstration of the principle, Figure 13 shows the values of pressure amplitude measured in an unsteady process (somewhere half way from the engine start-up towards a steady state condition) for three independent experiments carried out on three different dates. It can be seen that the spread of the results is within around 1% the pressure values. Similar values of repeatability/uncertainty can be associated with the power measurements in Figure 11 and temperature gradient measurements in Figure 12. In the latter case it is not the thermocouple “accuracy” that is decisive (0.1 K) but the repeatability of the independent experiments that indeed give the spread of temperature values within 1% range.

5. Conclusions

The motivation behind the current research is to identify the low cost regenerators with a possible comparable performance to those widely used in the thermoacoustic practice. Six different regenerators have been built and tested to compare the random wire regenerator with the mesh screen regenerators, as well as the regular geometry of the ceramic regenerator. The scourers and steel wool regenerators tested indicate a much worse performance in terms of both the onset temperature difference and the pressure amplitude compared with their wire-mesh screen counterparts of the same hydraulic radius. An exception here is a good performance of wire "wool" regenerator at elevated pressures. It can also be seen that the ceramic regenerator offers a reasonable performance (compared to wire screens), especially in the range of lower pressures (e.g. up to 5 – 6 bar).

However, when using alternative materials it is not always possible to keep all parameters the same – here it is clear that one of the parameters that could not be kept constant is the regenerator porosity. The measured results hint that the porosity and the flow resistance also affect the performance of the tested regenerators. The very high porosity of the scourers regenerators causes higher thermal relaxation loss. For the scourers regenerator, both the flow resistance and high porosity are the possible reasons leading to a very low performance. Therefore, it is clear that any future comparisons must not focus on the hydraulic radius alone, but possibly on other properties including porosity and physical properties of the regenerator material itself.

Furthermore, the investigation in this work also shows that the commercially available steel wool is usually quite fine in terms of equivalent wire diameter. To achieve a similar hydraulic radius, the porosity of the regenerator is usually quite high. However, the flow resistance increases quickly, when more steel wool is pressed into the can to get a relatively low porosity. Therefore, there should be a balance between the low flow resistance and sufficient material for heat transfer. More experimental work is required to better understand the relative performance of various regenerator materials. It would also be useful to control the wire sizes in a more systematic manner. One way to achieve this may be to use machining "swarf" of controlled wire sizes by controlling the machining processes itself.

It should also be noted that one of the motivations of this work is to compare the regenerators made out of different materials, with different geometrical configurations and different pore structure experimentally. However, as described in this paper, each regenerator has a different resistance, and hence the timing between velocity and pressure cannot be kept constant in the regenerators. The question arises: if the timing (phase shift) between pressure and velocity oscillations cannot be constant, to what extent, the experimental comparisons indicate the real difference in performance. On the other hand, it would also be interesting to find out how to control the phase by additional components in the acoustic network in order to keep the regenerators operating conditions comparable.

Acknowledgments

The authors wish to thank the Engineering and Physical Sciences Research Council UK for supporting this work under grants: GR/S26842/01, GR/T04502/01 (EPSRC Advanced Research Fellowship), GR/T04519/01 and EP/E044379/1 and the European Commission for funding under grant THATEA, reference number 226415.

References

[1] Backhaus S. and Swift G. W., "New varieties of thermoacoustic engines", *Proc. 9th International Congress on Sound and Vibration*, Orlando, USA, Paper number 502, July 8-11 2002.

[2] Matveev K. I., "Thermoacoustic energy analysis of transverse-pin and tortuous stacks at large acoustic displacements", *Int. J. Therm. Sci.*, Vol. 49, p. 1019, 2010.

[3] Rott, N., "Damped and Thermally Driven Acoustic Oscillations in Wide and Narrow Tubes", *Z. Angew. Math. Phys.*, Vol. 20, p. 230, 1969.

[4] Rott, N., "Thermally Driven Acoustic Oscillations, Part II: Stability Limit for Helium", *Z. Angew. Math. Phys.*, Vol 24, p. 54, 1973.

[5] Ceperley, P. H., "A Pistonless Stirling Engine – The Travelling Wave Heat Engine", *J. Acoust. Soc. Am.*, Vol. 66, p. 1508, 1979.

[6] Swift, G. W., "Thermoacoustic engines", *J. Acoust. Soc. Am.*, Vol. 84, p. 1145, 1988.

[7] Swift, G. W., "Analysis and Performance of a Large Thermoacoustic Engine", *J. Acoust. Soc. Am.*, Vol. 92, p. 1551, 1992.

[8] Olson, J. R., and Swift, G.W., "A Loaded Thermoacoustic Engine", *J. Acoust. Soc. Am.*, Vol. 98, p. 2690, 1995.

[9] Zhou, S., and Matsubara, Y., "Experimental Research of Thermoacoustic Prime Mover", *Cryogenics*, Vol. 38, p. 813, 1998.

[10] Ceperley, P. H., "Gain and Efficiency of a Short Travelling Wave Heat Engine", *J. Acoust. Soc. Am.*, Vol. 77, p. 1239, 1985.

[11] Yazaki, T., Iwata, A., Maekawa, T., and Tominaga, A., "Travelling Wave Thermoacoustic Engine in a Looped Tube", *Phys. Rev. Lett.*, Vol. 81, pp. 3128-3131, 1998.

[12] Yu Z., Backhaus S., and Jaworski A. J., "Design and testing of a travelling-wave looped-tube engine for low-cost electricity generators in remote and rural areas", *Proc. 7th Annual International Energy Conversion Engineering Conference*, paper AIAA-2009-4540, 2-5 August 2009.

[13] Backhaus, S., and Swift, G. W., "A Thermoacoustic-Stirling Heat Engine: Detailed Study", *J. Acoust. Soc. Am.*, Vol. 107, p. 3148, 2000.

[14] de Blok, C.M., "Low operating temperature integral thermoacoustic devices for solar cooling and waste heat recovery". *Proc. Acoustics'08*, Paris; 29 June–4 July, 2008.

[15] Yu, Z., and Jaworski, A. J., "Impact of acoustic impedance and flow resistance on the power output capacity of the regenerators in travelling-wave thermoacoustic engines", *Energy Conversion and Management*, Vol. 51, p. 350, 2010.

[16] Sugita, H., Matsubar, Y., Kushino, A., Ohnishi, T., Kobayashi, H., and Dai W., "Experimental Study on Thermally Actuated Pressure Wave Generator for Space Cryo-cooler, *Cryogenics*, Vol. 44, pp. 431–437, 2004.

[17] Gardner, D. L., and Swift, G. W., "A Cascade Thermoacoustic Engine", *J. Acoust. Soc. Am.*, Vol. 114, No. 4, pp. 1906-1919, 2003.

[18] de Blok, C. M., "Thermoacoustic System", *Dutch Patent*, International Application Number PCT/NL98/00515, 1998.

[19] Backhaus, S., and Swift, G. W., "Fabrication and Use of Parallel Plate Regenerators in Thermoacoustic Engine", *Proc. 36th Intersociety Energy Conversion Engineering Conference*, Savannah, Georgia, 29 July – 2 August, 2001.

[20] Backhaus, S., and Swift, G. W., "A Thermoacoustic Stirling Heat Engine", *Nature*, Vol. 399, p. 335, 1999.

[21] Swift, G. W., *Thermoacoustics, a Unifying Perspective for Some Engine and Refrigerators*, Acoustical Society of America, New York, 2002.

[22] Choi S., Nam K., and Jeong S., "Investigation on the pressure drop characteristics of cryocooler regenerators under oscillating flow and pulsating pressure conditions", *Cryogenics*, Vol. 44, Issue 3, pp. 203-210, 2004.

[23] Nam K., and Jeong s., "Measurement of cryogenic regenerator characteristics under oscillating flow and pulsating pressure". *Cryogenics*, 43 (10), pp. 575–581, 2003.

[24] Appel H., and Eder F.X., "Pressure drop in selected porous materials used for thermal regenerators", *Cryogenics*, Vol. 20, Issue 10, pp. 587-591, 1980.

[25] Fusco, A. M., Ward, W. C., and Swift, G. W. "Two-sensor Power Measurements in Lossy Ducts", *J. Acoust. Soc. Am.*, Vol. 84, pp. 2229-2235, 1992.

[26] Atchley A. A., and Kuo F. M., "Stability curves for a thermoacoustic prime mover", *J. Acoust. Soc. Am.*, Vol. 95, Issue 3, pp. 1401-1404, 1994.

[27] Yu Z. B., Li Q., Chen X., Guo F. Z., Xie X. J., and Wu J. H., "Investigation on the oscillation modes in a thermoacoustic Stirling prime mover: mode stability and mode transition", *Cryogenics*, Vol. 43, pp. 687–691, 2003.

[28] Yu Z. B., Li Q., Chen X., Guo F. Z., and Xie X. J., "Study on the optimal characteristic dimension of regenerator in a thermoacoustic engine", *Proceedings of the Twentieth International Cryogenic Engineering Conference (ICEC20)*, pp. 357-360, 2005.

[29] Yu Z. B., Li Q., Chen X., Guo F. Z. and Xie X.J., "Experimental investigation on a thermoacoustic engine having a looped tube and resonator", *Cryogenics*, Vol. 45, Issue 8, pp. 566-571, 2005.

[30] Penelet G., Job S, Gusev V., Lotton P., and Bruneau M., "Dependence of Sound Amplification on Temperature Distribution in Annular Thermoacoustic Engines", *Acta Acoustica united with Acustica*, Vol. 91, pp. 567-577, 2005.

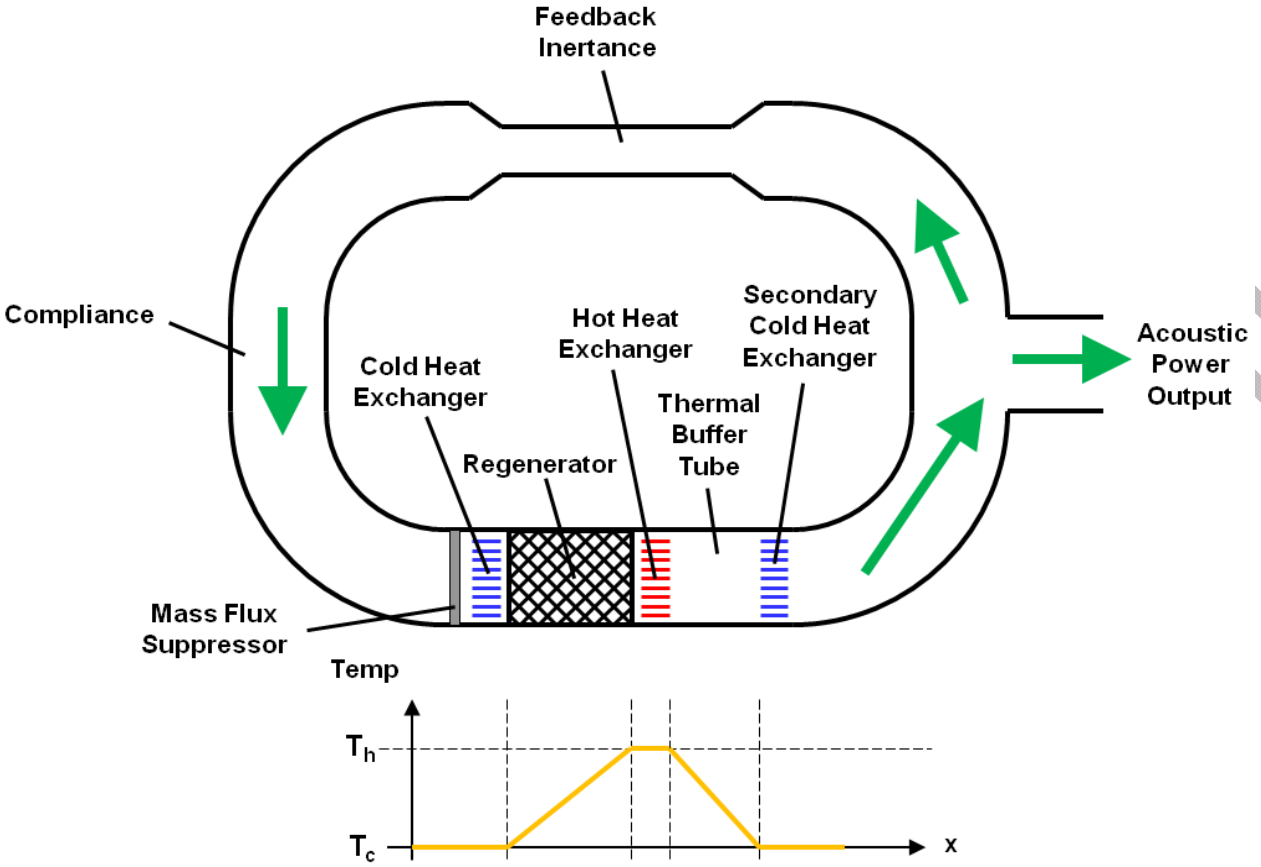

Figure 1 Schematic of a travelling wave thermoacoustic engine. The regenerator works as an acoustic power amplifier. Part of the acoustic power is extracted from the loop, part is returned for further amplification. Temperature distribution along the regenerator and associated heat exchangers is shown at the bottom.

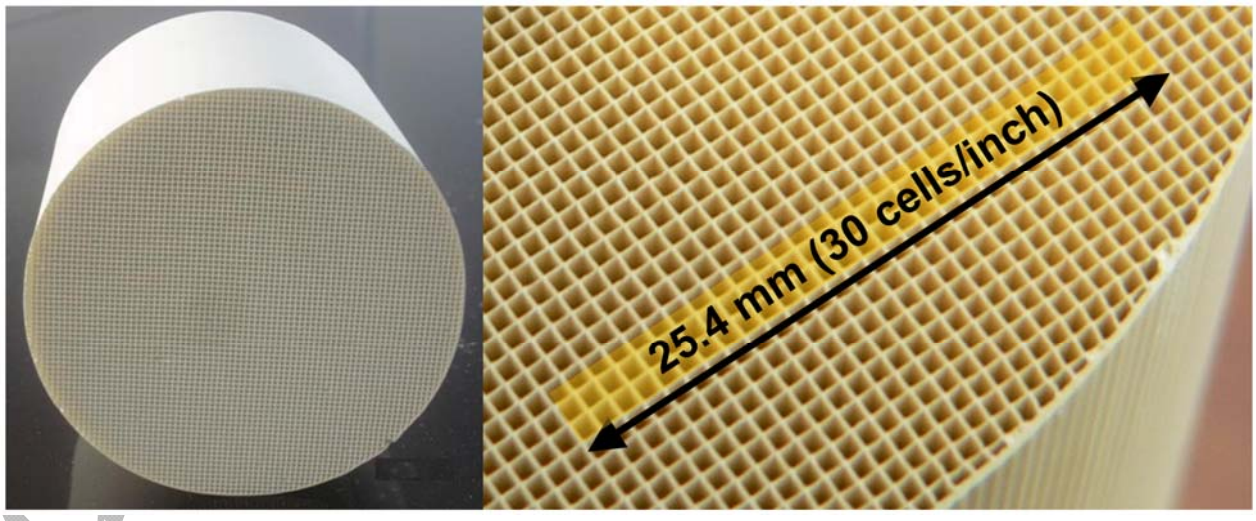

Figure 2 Image of ceramic substrate with square pores; whole sample of 75 mm diameter (left) and close-up of the structure of the pores (right).

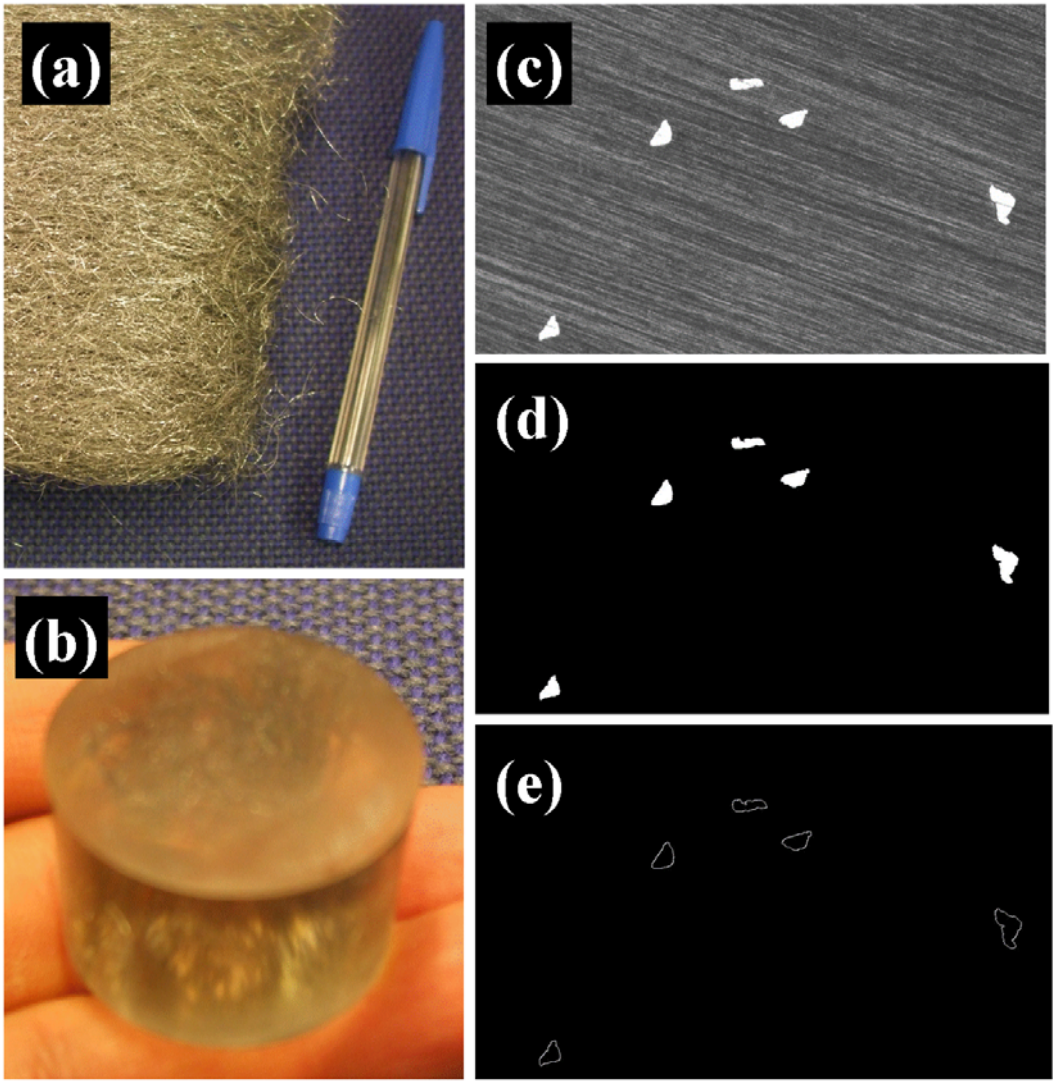

Figure 3 Characterisation of steel wool sample : (a) sample as purchased; (b) 300 random wires cast in epoxy mould; (c) a sample microscope image; (d) black and white image obtained by threshold techniques; (e) transformed image for estimating wire perimeters.

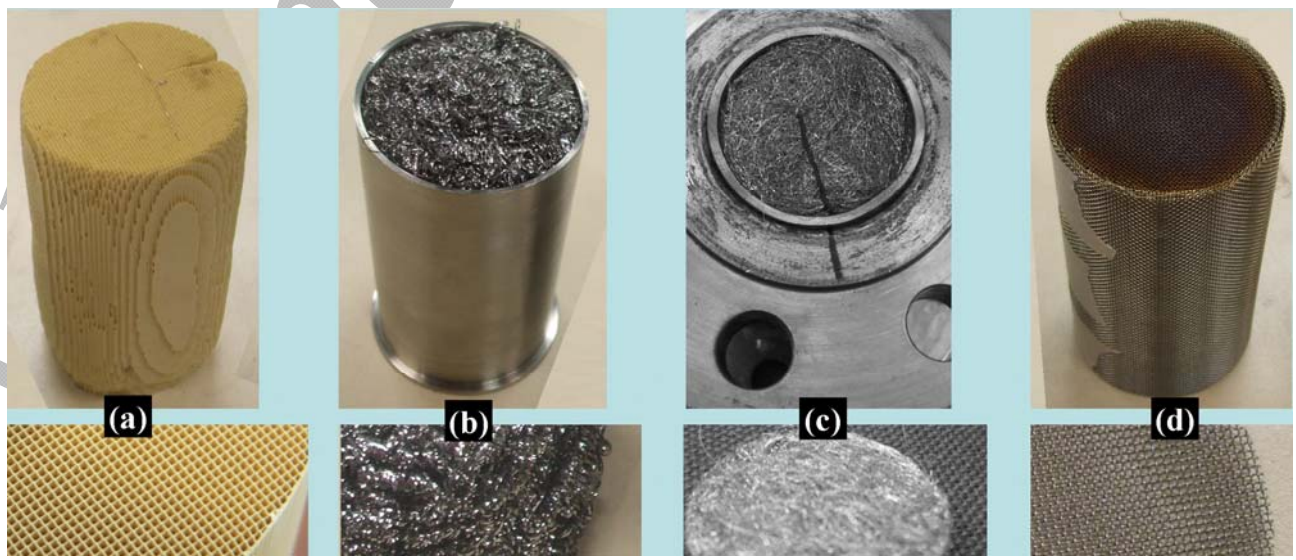

Figure 4 Actual regenerator setups and close-ups of materials (insets): (a) ceramic catalyst support (type I); (b) steel "scourers" (type II); (c) stainless steel "wool" (type III) and (d) wire mesh screens (type IV)

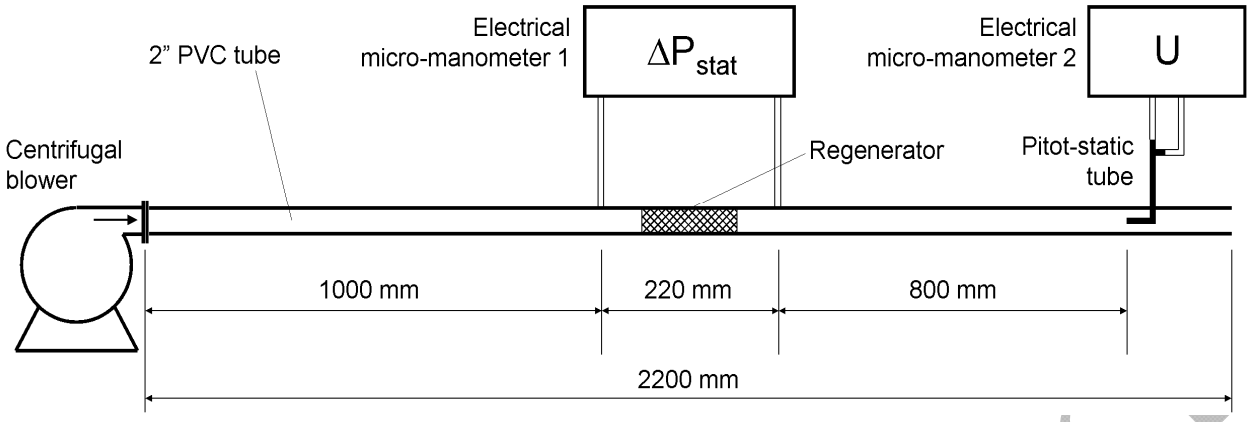

Figure 5 Experimental set up for static pressure drop measurements

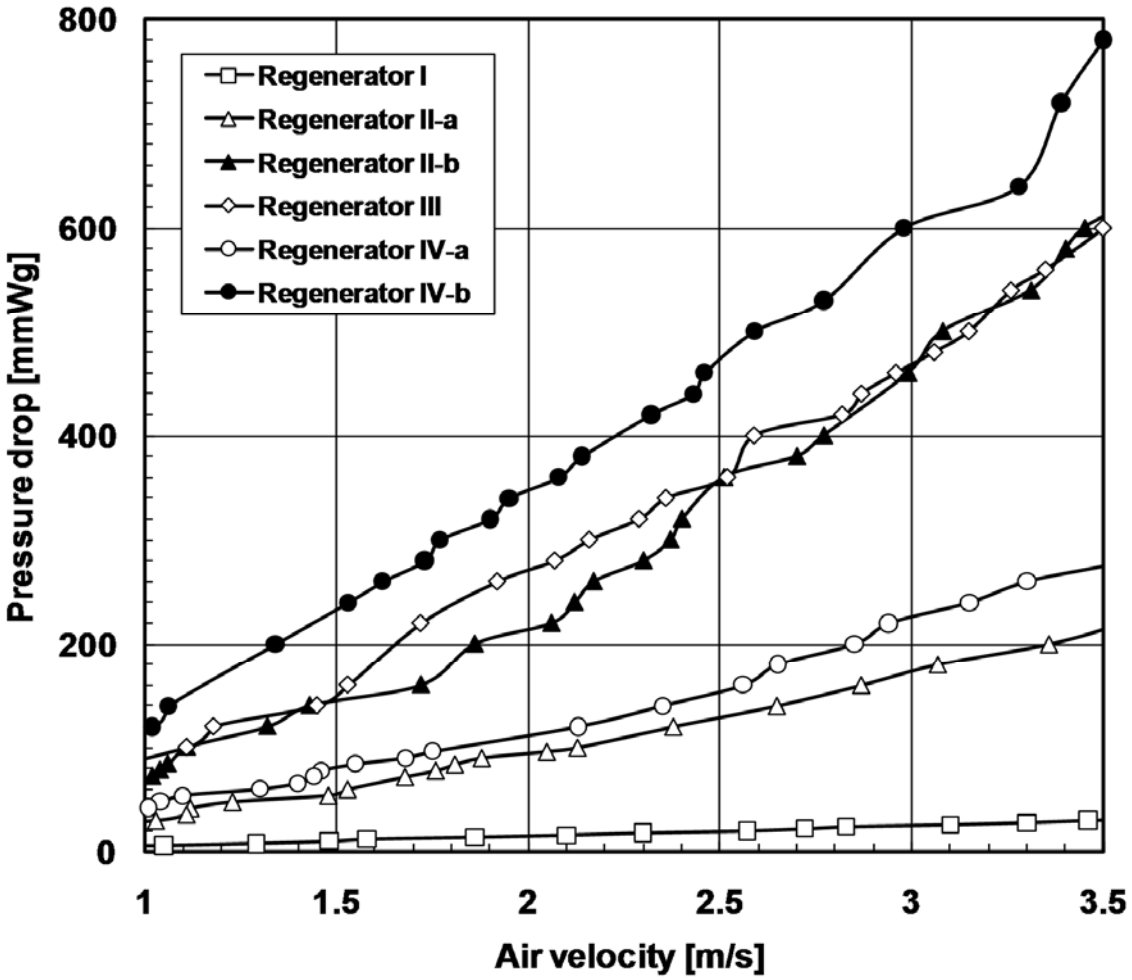

Figure 6 Results of static pressure drop measurements

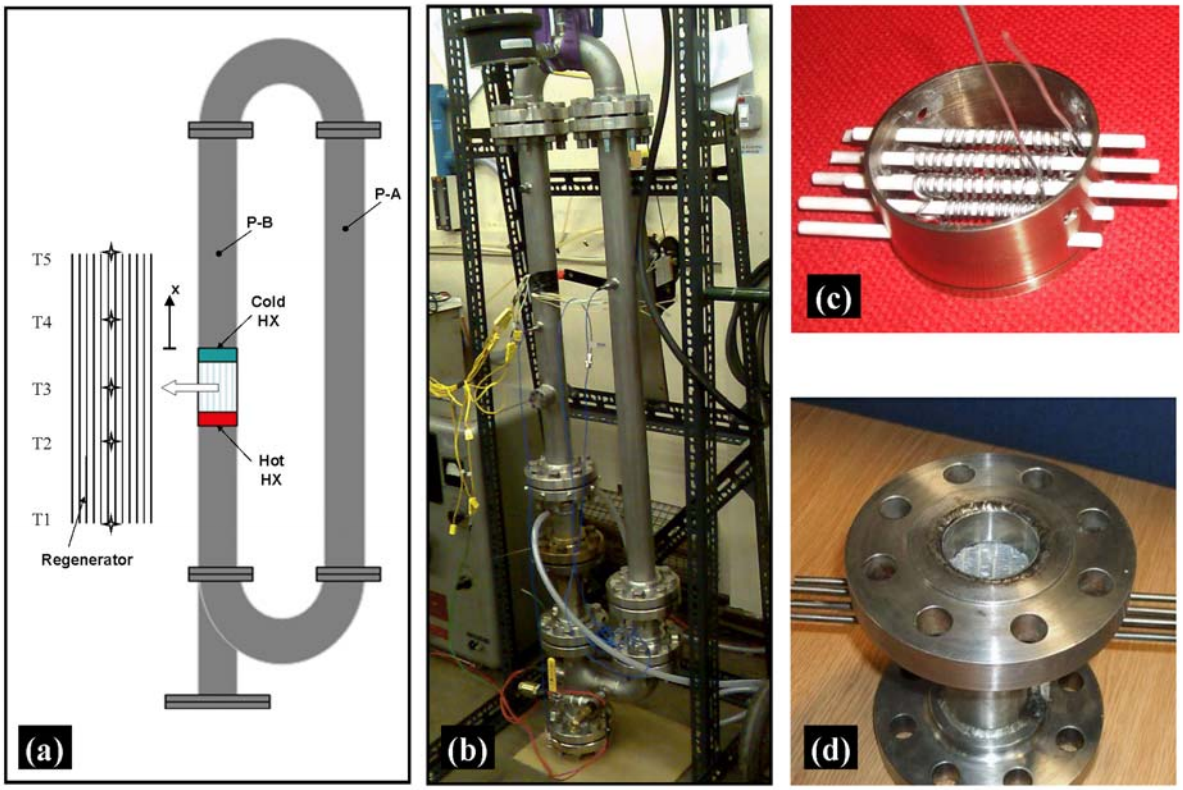

Figure 7 Experimental set up: (a) schematic diagram of the thermoacoustic engine showing measurement locations of thermocouples and pressure sensors; (b) image of the actual system; (c) hot heat exchanger; (d) cold heat exchanger.

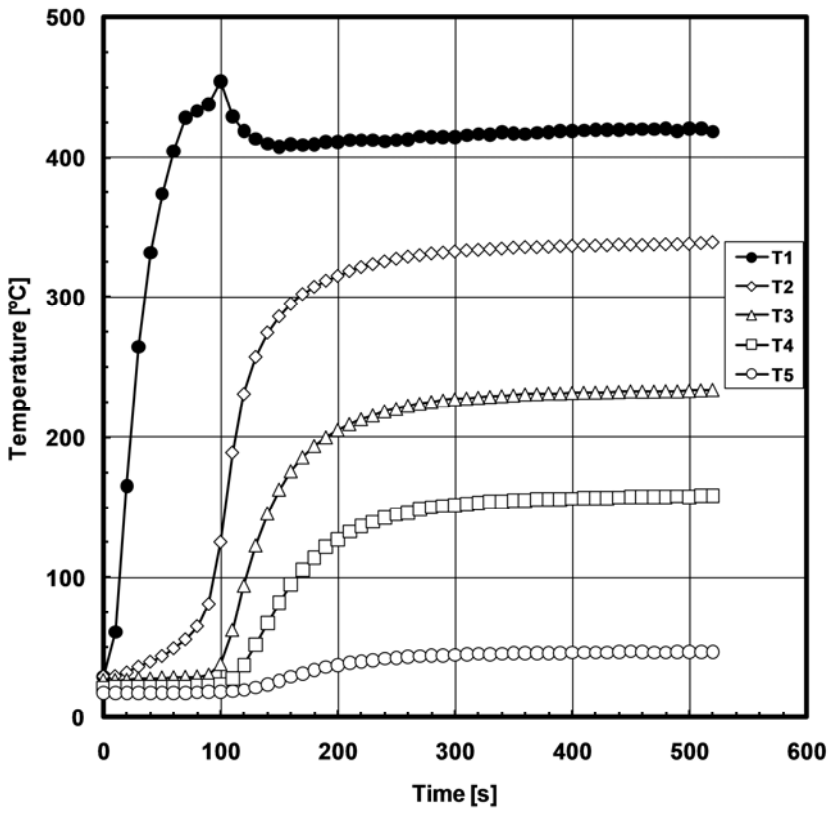

Figure 8 Example of unsteady temperature rise along Regenerator I during the onset experiments. Mean pressure is 4.4 bar.

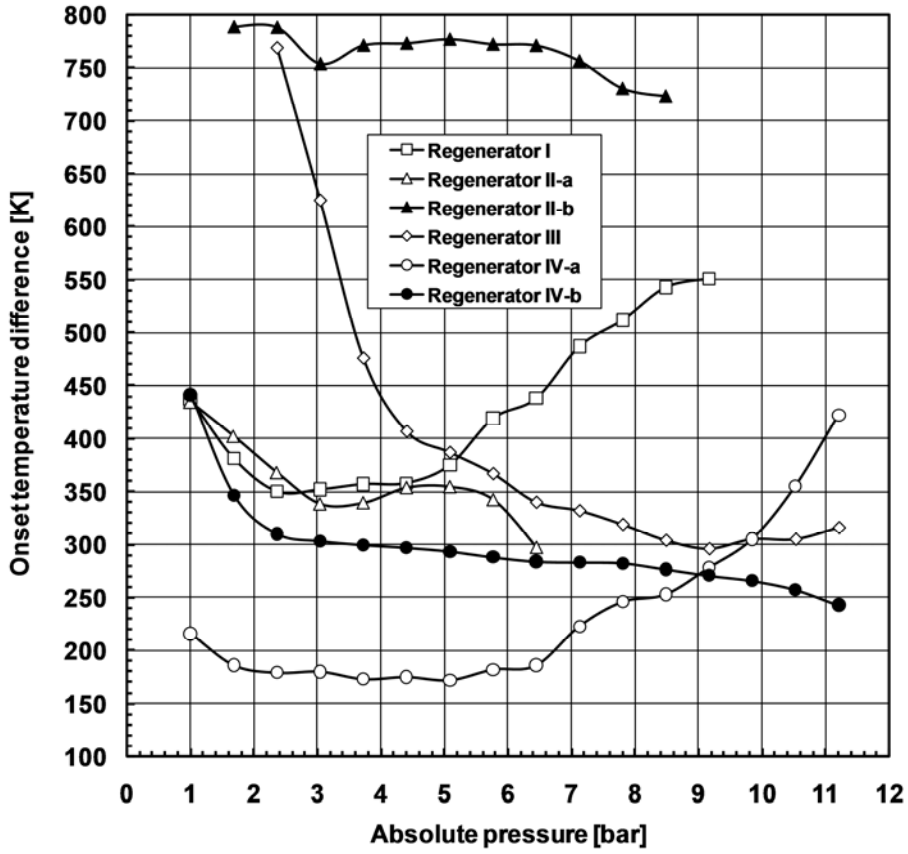

Figure 9 Onset temperature difference for all regenerators as a function of the mean working gas pressure

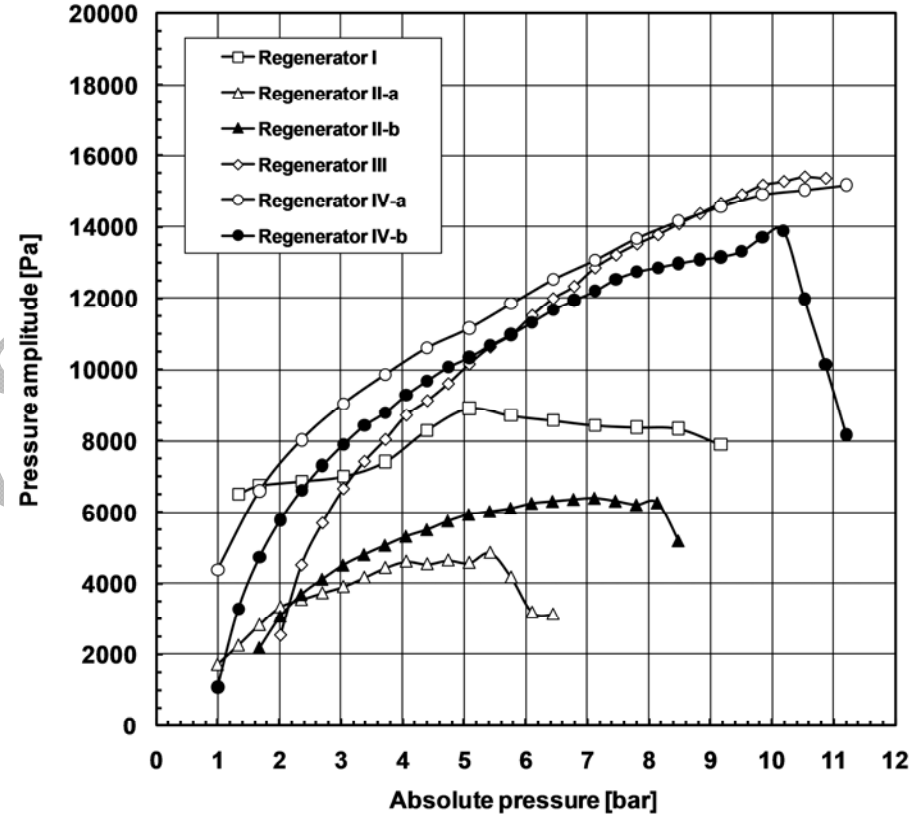

Figure 10 Acoustic pressure amplitude at location P-A for all regenerators

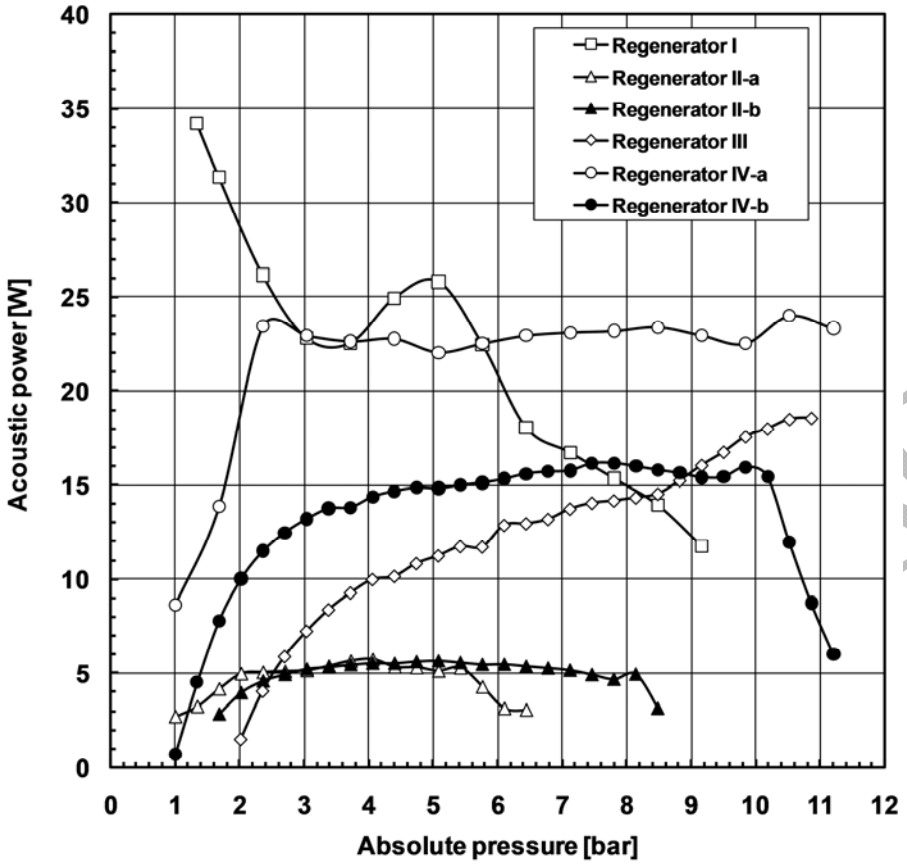

Figure 11 Estimated acoustic power passing through the middle point between P-A and P-B (cf. Fig 7a).

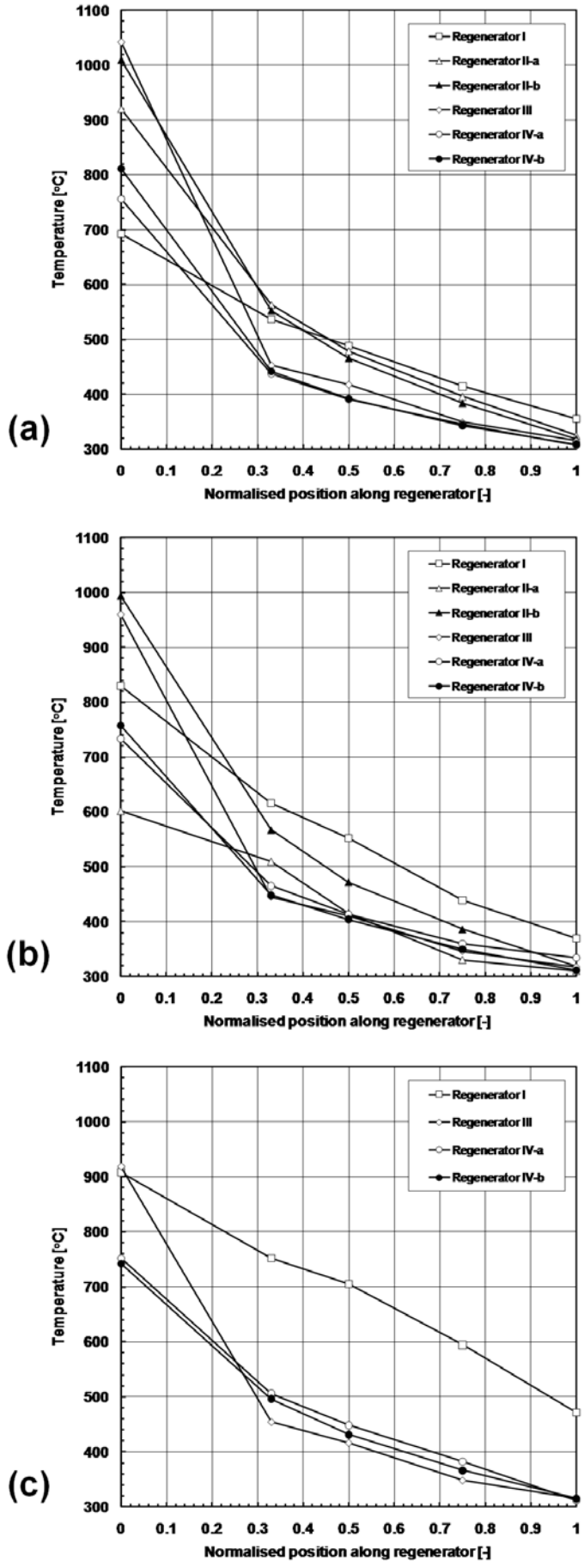

Figure 12 Temperature profiles inside the regenerators for selected mean pressures: (a) 3.04 bar; (b) 5.08 bar; (c) 9.16 bar (note at 9.16 bar not all engines would start – only 4 curves can be drawn).

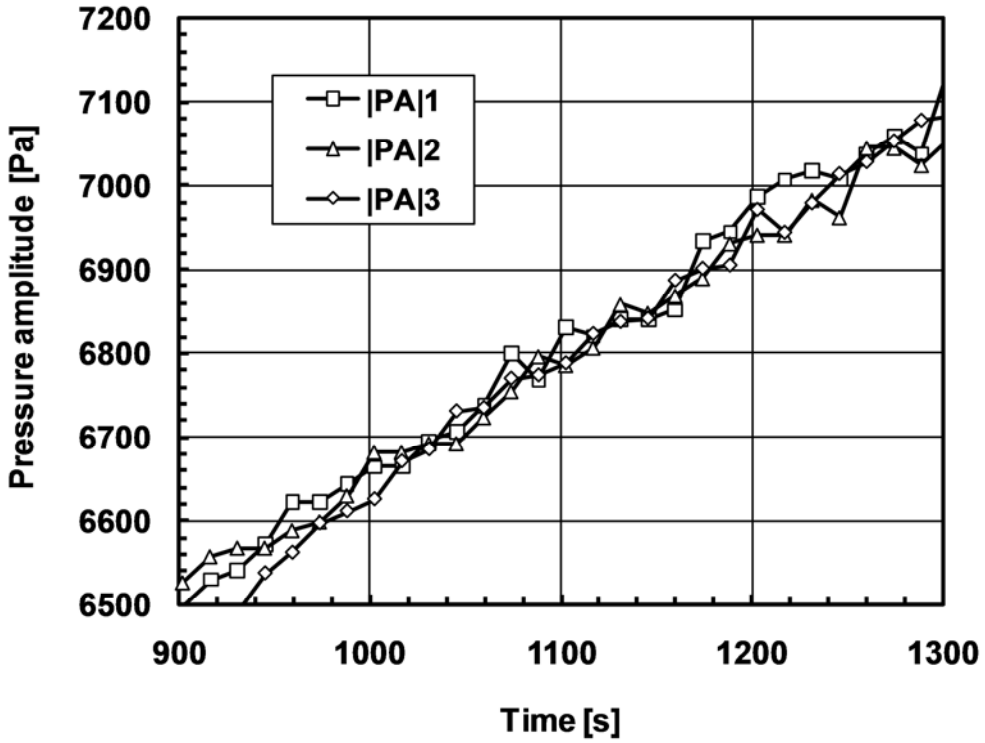

Figure 13 Illustration of the experimental uncertainty through repeatability test results. Pressure amplitude for is measured in an unsteady engine start-up process. Ceramic regenerator; 5.76 bar

Table 1 Summary of materials used for constructing all six regenerators

Symbol	Type of material used	Material Specifications		Porosity, %	Hydraulic radius, μm
		Mesh number	D_{wire}, μm		
I	Ceramic substrate	Corning cellular ceramic catalyst support		88.7	199
II-a	Steel "scourers"	Rectangular wire: 432 μm x 25.6 μm		94.2	200
II-b	Steel "scourers"	Rectangular wire: 432 μm x 25.6 μm		90.7	120
III	Stainless steel "wool"	Irregular wire average A_{cs} = 4570 μm^2; average P = 249 μm		91.6	200
IV-a	Wire mesh screens	30	280	72.7	196
IV-b	Wire mesh screens	45	230	67.5	121